Discovering Dark Matter with the MUonE Experiment

Gordan Krnjaic ©,[1, 2, 3, *] Duncan Rocha ©,[1, 4, †] and Isaac R. Wang ©[1, ‡]

[1] *Theoretical Physics Division, Fermi National Accelerator Laboratory, Batavia, IL, USA*
[2] *Department of Astronomy & Astrophysics, University of Chicago, Chicago, IL USA*
[3] *Kavli Institute for Cosmological Physics, University of Chicago, Chicago, IL USA*
[4] *Department of Physics, University of Chicago, Chicago, IL USA*
(Dated: September 6, 2024)

The MUonE experiment aims to extract the hadronic contribution to the muon anomalous magnetic moment from a precise measurement of the muon-electron differential scattering cross section. We show that MUonE can also discover thermal relic dark matter using only its nominal experimental setup. Our search strategy is sensitive to models of dark matter in which pairs of pseudo-Dirac fermions are produced in muon-nucleus scattering in the target, and the heavier state decays semi-visibly to yield dilepton pairs displaced downstream from the interaction point. This approach can probe sub-GeV thermal-relic dark matter whose cosmological abundance is governed by the same model parameters that set the MUonE signal strength. Furthermore, our results show that the downstream ECAL plays a key role in rejecting backgrounds for this search, thereby providing strong motivation for the MUonE to keep this component in the final experimental design.

Introduction. There has recently been great interest in developing new search strategies for dark matter discovery at fixed target accelerators involving proton [1, 2], electron [3], and muon [4] beams – see Refs. [5, 6] for detailed summaries. Collectively, these efforts aim to probe models in which sub-GeV DM achieves a thermal relic abundance through direct annihilation to Standard Model (SM) final states, such that the signal strength in the laboratory is governed by the same parameters that set the DM cosmological abundance.

The proposed MUonE experiment at CERN [7, 8] aims to measure the angular distribution of elastic muon-electron scattering to extract the hadronic contribution to the muon anomalous magnetic moment [9]. In this setup, a 160 GeV muon beam impinges on a series of thin, beryllium target modules surrounded by layers of tracking material. When muons upscatter stationary electrons in these targets, the angular trajectories of final state particles can be resolved within ~ 0.02 mrad. This capability also makes MUonE an excellent probe of new forces in muon-electron [10, 11] or muon-nucleon [12] scattering, provided that the force carriers decay to yield displaced vertices sufficiently far from the tungsten target layers.

In this *Letter*, we show for the first time that MUonE can be sensitive to thermal relic dark matter without any modifications to the proposed experimental design. Our benchmark scenario is a model of inelastic DM in which a pseudo-Dirac fermion pair with unequal masses couple to a kinetically mixed dark photon [13]. The heavier of these states is unstable and decays semi-visibly to yield displaced tracks of charged particles on laboratory length scales. At MUonE, both states are radiatively produced in muon-nucleus interactions inside the target layers and the heavier state decays in the forward direction

---
* krnjaicg@fnal.gov
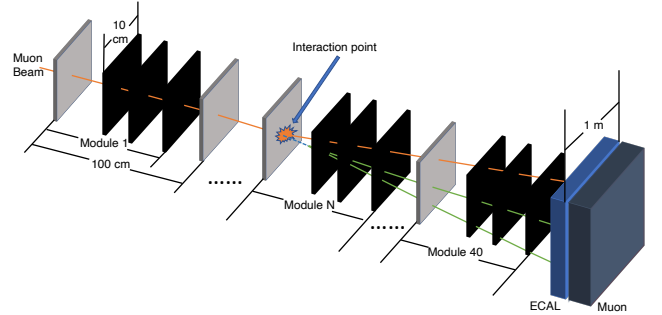† drocha@uchicago.edu
‡ isaacw@fnal.gov

FIG. 1. Schematic diagram of inelastic dark matter production in muon-nucleus scattering at the MUonE experiment. An incoming 160 GeV muon beam (orange line) scatters a beryllium nucleus at the interaction point and produces pseudo-Dirac dark states χ_1 and χ_2 through the processes depicted in Fig. 2. The heavier of these states decays semivisibly via $\chi_2 \to \chi_1 \ell^+ \ell^-$ such that the dileptons (green lines) emerge from a displaced vertex. Here the gray sheets represent the target material and the black sheets are tracking layers. The downstream ECAL serves to reject SM background processes.

to yield missing energy and dilepton pairs downstream in the tracking layers as depicted schematically in Fig. 1.

Inelastic Dark Matter. The inelastic dark matter was first proposed to resolve the DAMA anomaly [13]. A pair of pseudo-Dirac fermions χ_1 and χ_2 are proposed with a small mass splitting Δ. They couple to a kinetically mixed dark photon A' with an off-diagonal interaction

$$\mathcal{L}_{\text{int}} = -\epsilon e A'_\mu J^\mu_{\text{EM}} - (g_D A'_\mu \overline{\chi}_2 \gamma^\mu \chi_1 + h.c.) , \quad (1)$$

where A' is a massive "dark photon" mediator with mass $m_{A'}$ and kinetic mixing parameter ϵ, J_{EM} is the SM electromagnetic current, and the $\chi_{1,2}$ have masses $m_{1,2}$ with splitting $\Delta \equiv m_2 - m_1$. The off-diagonal coupling $A' \chi_2 \gamma^\mu \chi_1$ in Eq. (1) can naturally arise if a four-
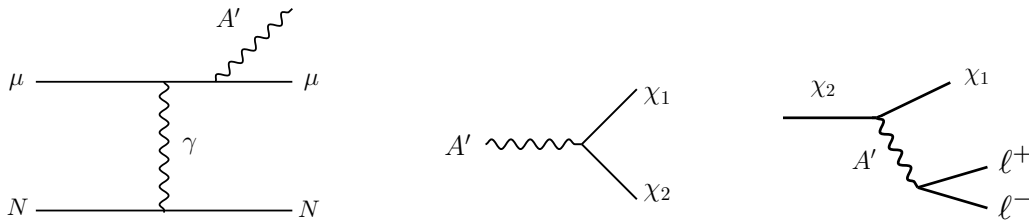
FIG. 2. Feynman diagrams representing the sequence of steps that yield the inelastic DM signal at MUonE. **Left:** a dark photon A' is radiatively produced in μ-N scattering, where N is a Be nucleus. **Middle:** the A' decays through the off-diagonal coupling to the pseudo-Dirac fermions. **Right:** for $\Delta < m_{A'}$, the heavier state decays via $\chi_2 \to \chi_1 \ell^+ \ell^-$ to yield a displaced dilepton pair downstream of the interaction point at MUonE.

component fermion has a Dirac mass and a Majorana mass in the interaction basis, such that its vector current with A' is off-diagonal in the mass eigenbasis $\chi_{1,2}$[13].

In the predictive parameter space of interest,[1] $g_D \gg e\epsilon$ and $m_{A'} > m_1 + m_2$, so the dark branching fraction satisfies $\mathrm{Br}(A' \to \chi_1\chi_2) \approx 1$. If $\Delta < m_{A'}$, the unstable heavier state decays via $\chi_2 \to \chi_1 \bar{f} f$ where, for each f channel, which corresponds to the decay length[2]

$$\frac{c\tau}{\gamma} \approx 10\,\mathrm{cm} \left(\frac{m_{A'}}{10^2\,\mathrm{MeV}}\right)^4 \left(\frac{20\,\mathrm{MeV}}{\Delta}\right)^5 \left(\frac{10^{-7}}{\epsilon^2\alpha_D}\right),$$

where γ is the boost factor and we have taken the massless f limit. In principle f here could be any fermion, but for the Δ of interest here, most of the MUonE signal arises from $\chi_2 \to \chi_1 \ell^+\ell^-$ decays, where $\ell = e, \mu$.

In the early universe at temperatures $T \gg m_{1,2}$, the $\chi_{1,2}$ maintain chemical equilibrium with the SM through $\chi_1\chi_2 \leftrightarrow \bar{f}f$ coannihilation through virtual A' exchange, where f is a charged SM fermion. In the $m_{A'} \gg m_1 \gg \Delta, m_f$ limit, the annihilation cross section times velocity for a single f final state scales as [2]

$$\sigma v \propto \frac{\epsilon^2\alpha_D m_1^2}{m_{A'}^4} \equiv \frac{y}{m_1^2} \ , \ y \equiv \epsilon^2\alpha_D \left(\frac{m_1}{m_{A'}}\right)^4, \qquad (2)$$

where y is a dimensionless interaction strength parameter and, in the same limit, the relic density satisfies [15]

$$\Omega_{\chi_1} + \Omega_{\chi_2} \sim 0.1 \left(\frac{y}{10^{-10}}\right) \left(\frac{100\,\mathrm{MeV}}{m_1}\right)^2. \qquad (3)$$

For the larger (order unity) mass splittings we consider here, the relic density is obtained by numerically solving the Boltzmann equations for this system, as done in Refs.

[2, 14, 16, 17] and we use these curves from Ref. [16] for comparison with the MUonE sensitivity.

After $\chi_{1,2}$ chemically decouple from the SM, the heavier χ_2 state is further depleted via decays, so that for $T \ll \Delta$, the dark sector consists of χ_1 particles and no χ_2 coannihiltion partners. Thus, during the CMB epoch, this model evades limits on late-time energy injection, which otherwise rule out thermal relics with mass below 20 GeV [18]. In the present day universe, χ_1 constitutes all of the cosmological and galactic dark matter. For a detailed discussion of this model, its cosmological history, and various experimental constraints, see Refs. [14–16, 19, 20]

The MUonE Experiment. Inspired by NA7 experiment [21, 22], MUonE aims to extract the running α by precisely measuring the differential $\mu^\pm e^- \to \mu^\pm e^-$ cross section [7, 8]. This running can be used to extract the hadronic vacuum polarization contribution to muon anomalous magnetic magnetic moment [23, 24], which is crucial to resolving the longstanding discrepancy between theory [25, 26] and experiment [9, 27, 28]. For an up-to-date status report on MUonE, see Ref. [29].

MUonE plans to deliver a 160 GeV muon beam from the CERN M2 beamline onto a series of 40 target modules. Each module consists of one 15 mm Be sheet and three downstream tracking layers with $10 \times 10\,\mathrm{cm}^2$ cross-sectional area. Within each module, the first tracking layer is positioned 15 cm behind the target. The exact location of the 2nd and 3rd tracking layers has not been fully decided yet. In this work, we apply 1 meter as the distance from the target to the 3rd tracking layer as a conservative selection criterion for angular acceptance and assume the 2nd tracking layer stands at the middle point between the 1st one and the 3rd one. The target modules are spaced 1 m apart from each other along the beamline and this setup is expected to achieve an integrated luminosity of $\mathcal{L} = 1.5 \times 10^4$ pb^{-1} for μ-e scattering, corresponding to $\sim 10^{16}$ muons on target.

To achieve high measurement accuracy, MUonE employs a CMS-based tracking apparatus [8, 30, 31], which can resolve the angle resolution of outgoing particles to within 0.02 mrad. There is no applied magnetic field, so the trajectories of outgoing charged particles are not bent

---

[1] in the opposite regime where $\epsilon e \gtrsim g_D$, achieving the observed relic abundance requires large values of ϵ that are largely excluded by existing experiments. Furthermore, if $m_{A'} < m_1+m_2$, the relic abundance arises from $\chi_i\chi_i \to A'A'$ annihilation, and does not depend on ϵ which governs accelerator production.

[2] Here we have used the fact that the χ_2 rest frame lifetime satisfies $\tau^{-1} = 15\pi m_{A'}^4/(4\epsilon^2\alpha\alpha_D\Delta^5)$ [14]

Variable	Selection Criteria
Decay z coordinate	$25\,\text{mm} < z < 140\,\text{mm}$
Decay daughter energy	$> 5\,\text{GeV}$
Decay daughter opening angle	> 1 mrad
Charged track geometry	Hit all 3 trackers
Modules	Last 5

TABLE I. Event selection criteria for our proposed search. In our numerical results, these requirements are imposed on our signal and background MC events.

as they traverse the beamline. Note that the experimental setup is not designed to measure the outgoing energies or momenta of any charged particles passing through the instrumented region.

Behind the last target module, there is a proposed electromagnetic calorimeter (ECAL), followed by a muon filter system. The precise particle identification (PID) efficiency and overall size of this combined system have not yet been finalized, but its cross-sectional area is expected to be of order 1×1 m^2 [8]; for concreteness, here we assume this area is 1×1 m^2. In Fig. 1, we show a schematic design of MUonE experiment with particle trajectories representing our inelastic DM signal process.[3]

Dark Matter Signal. In our scenario, the MUonE signal arises from the steps depicted in Fig. 2 and corresponds to the sequence

$$\mu N \rightarrow \mu N A' \ , \quad A' \rightarrow \chi_1 \chi_2 \ , \quad \chi_2 \rightarrow \chi_1 \ell^+ \ell^-, \quad (4)$$

where N is a beryllium nucleus in the target. Since the χ_1 is invisible, the downstream signal arises purely from χ_2 decays, which generically yield a displaced vertex in our parameter space of interest. Since $c\tau \propto m_{A'}^4/(\Delta^5 \epsilon^2 \alpha_D)$ from Eq. (2), even mild hierarchies in the $m_{A'}/\Delta > 1$ ratio can yield macroscopic displacements. Note that the same model parameters that govern the dark matter relic density also set the signal strength at MUonE, and therefore provide an experimental milestone for discovering or falsifying this scenario in the laboratory.

The signal topology from Eq. (4) consists of one primary muon track, and two additional charged tracks originating from the same displaced vertex. We also require that all three tracks in the event pass through all three tracking layers in their module of origin to ensure high event reconstruction efficiency. Two of these charged tracks must be reconstructed from a common displaced vertex between the target and the first tracking layer. These displaced tracks must also have an opening angle larger than 1 mrad to successfully reconstruct the displaced vertex [32]. As we will see in the next section, the two tracks from the displaced vertex must

---

[3] Unlike the cartoon in Fig. 1, the nominal MUonE signal of interest would consist of only one muon track and one electron track downstream of the interaction point
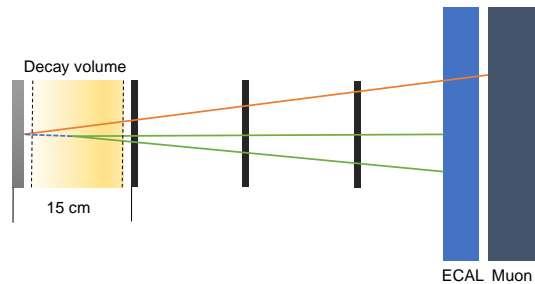

FIG. 3. A schematic depiction of the inelastic DM signal in one MUonE target module. Here the red track is the beam muon and the green tracks which reconstruct a displaced vertex are the additional charged tracks from the displaced $\chi_2 \rightarrow \chi_1 \ell^+ \ell^-$ decay. We require that the χ_2 decay occur within the ~ 15 cm fiducial decay volume (shaded yellow), whose longitudinal endpoints satisfy the inequalities in Eq. (5)

be either an e^+e^- or $\mu^+\mu^-$ pair in order to reject SM backgrounds with the PID system. The primary muon must also be identified by the ECAL and the Muon filter, as in the original proposal of the MUonE experiment. Given the expected z-direction spatial resolution $\delta z \simeq 1$ mm [10, 32], we further require that this displaced vertex is at least $10\delta z$ away from both the target and the first tracking layer. Thus, we require that the longitudinal endpoints of the fiducial χ_2 decay region satisfy

$$25 \text{ mm} \leq z_{\chi_2 \text{ decay}} \leq 140 \text{ mm}, \quad (5)$$

as measured from the interaction point within a given target module. In Fig. 3, we show a schematic overhead view of a signal event whose final state tracks satisfy our geometric selection criteria.

Beyond geometry, we must also ensure that these tracks correspond precisely to the particles from our signal prediction (one beam muon and two displaced dileptons), as opposed to fakes from other particles. Furthermore, we must also ensure that no additional neutral hadrons are produced in association with three charged tracks, as our scenario predicts no additional hadronic activity in the final state. For these purposes, the ECAL and Muon system at the end of the beam line are essential for vetoing backgrounds. For example, if the displaced tracks arise from charged pions instead of electrons, the energy deposited in the ECAL can discriminate between these cases and the absence of muons in the Muon system can rule out the possibility that the displaced tracks arise from dileptons. Alternatively, even if a given event has exactly one beam muon and a displaced dilepton pair, if there are additional energy deposits in the ECAL that do not correspond to any charged tracks (e.g. from a neutral pion), it can also be vetoed as background.

However, as particles lose energy traversing the tracking layers, the ECAL PID capability can deteriorate, thereby reducing its ability to veto backgrounds. Muon
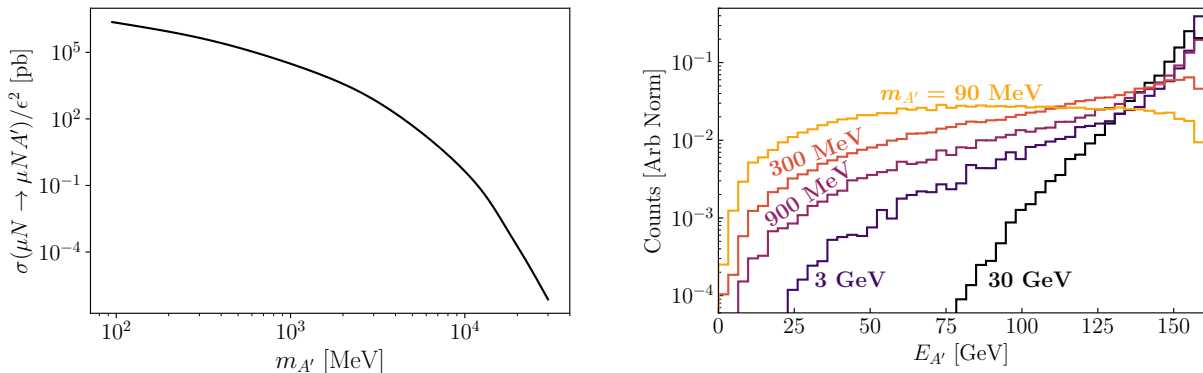
FIG. 4. **Left:** Cross section for dark photon production via the bremmstrahlung-like process $\mu N \to \mu N A'$ at MUonE, where N is a beryllium nucleus, calculated using `CalcHEP`. **Right:** Recoiling A' energy distribution from the same simulation sample prior to any event selection.

and electron can scatter off the material when penetrating the targets and the tracking layers in each module before it arrives the ECAL. To mimic the detector response of the tracking layers and the ECAL, as discussed in Ref. [10] based on details of energy loss [33, 34], we consider a conservative[4] energy threshold of $E > 5$ GeV for each of the three charged tracks. For the same reason, only the last 5 modules are considered in this work to ensure sufficiently high ECAL PID efficiency; events originating in modules further upstream risk significant energy loss from the other 35 target and tracking modules. Furthermore, since the ECAL has a large surface area, charged tracks with energy above the energy threshold are guaranteed to enter the ECAL if they pass through the three tracking stations for these last 5 modules. We summarize our full selection criteria in Table I.

Signal Simulation. To compute the number of expected signal events in MUonE, we use `FeynRules` [35] to construct the inelastic dark matter model. We then use `CalcHEP 3.8.9` [36] to generate Monte Carlo (MC) events for $(\mu^- \text{Be} \to \mu^- \text{Be} A')$ with a muon beam energy of 160 GeV and kinematic distributions for the $\chi_2 \to \chi_1 e^+ e^-$ and $\chi_2 \to \chi_1 \mu^+ \mu^-$ decay channels. For each point, we generate 50k signal events. The production events are then are re-weighted according to the nuclear form factor of beryllium (an analytic formulation of this process is described in [37]). These events are then filtered through the series of cuts discussed in the previous section and listed in Table I.

In Fig. 4 we show distributions of A' production in our signal simulation. The left panel shows the total cross section for $\mu N \to \mu N A'$ production normalized to $\epsilon = 1$ and the right panel shows the energy distribution of recoiling muons following A' production for various values

of $m_{A'}$. In Fig. 5 we also show energy angle distribution histograms for the simulated χ_2 produced in $A' \to \chi_1 \chi_2$ decays at MUonE.

Background Simulation. SM events that fake our signal fall into two distinct categories:

- **Mis-reconstructed events:** backgrounds can arise from SM events with charged tracks that originate within the target, but are mis-reconstructed as displaced vertices. This category also includes events in which SM particles produced inside the target interact later to generate additional $e^+ e^-$ tracks within the downstream tracking layers. By requiring the decay volume to have a 10 δz displacement away from both the target and the first tracking layer, this category of events can be safely rejected [10, 32].

- **Long lived hadrons:** genuine displaced vertex can arise from long-lived hadrons that decay to yield dileptons in between the target and first tracking layer. These particles are produced in inelastic muon-nucleon scattering and decay downstream of the target to yield high multiplicities of charged tracks (more than two charged tracks plus the beam muon), which can easily be vetoed.

To estimate the number of background events from the second category, we run `Pythia 8.307` [38] to simulate muon-nucleon scattering at MUonE. The muon-nucleon scattering can be categorized by Q^2, the momentum tranfer to the nucleus. A large Q^2 corresponds to deep-inelastic scattering (DIS), which can be modeled using perturbative QCD, and in this regime, the muon deflection angle has a minimum value. Below this threshold, soft QCD production dominates, in which case the muon deflection angle is bounded from above.

We generate 1.5×10^{10} soft QCD events and 6×10^8 deep-inelastic scattering (DIS) events; both samples greatly exceed the expected number of such events in

---

[4] This requirement was based on internal communication [32] and was applied as the most conservative choice in one of the previous study [10]
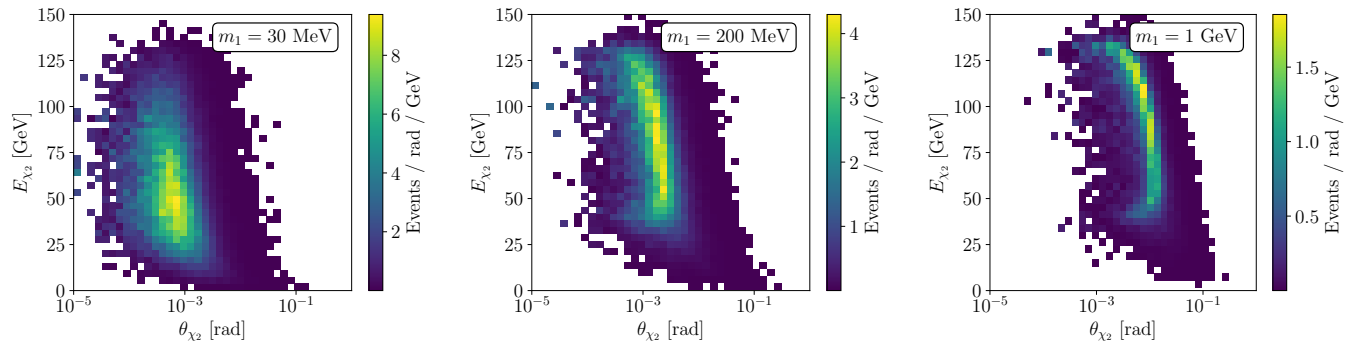
FIG. 5. Energy angle distributions for χ_2 from our simulation of $\mu N \to \mu N A'$ scattering, followed by $A' \to \chi_1 \chi_2$ decays at MUonE for various values of m_1 assuming $\Delta = 0.4 m_1$, prior to any event selection.

each category for the MUonE luminosity.[5] The minimum simulated Q^2 delivered to the target for DIS (a free parameter in Pythia) is chosen so that the differential cross section for hadroproduction is continuous across the soft-QCD and DIS kinematic regimes.

Using these samples, we veto any simulated SM events that contain tracks beyond the three that can fake our signal topology (one track from the beam muon and two displaced tracks from the dilepton pair). Such additional tracks can arise from charged particles with energies above the 5 GeV lepton energy threshold (see Table I). In addition, any neutral particles above this energy threshold (except neutrinos) can be detected and vetoed using the downstream ECAL. Importantly, we find that this conclusion is insensitive to the choice of energy threshold, varying from 10 MeV to 5 GeV. Note that the vast majority of the background events from hadronic processes arise from $K^0 \to \pi^+ \pi^-$ or $\Lambda \to p \pi^-$ decays. In these cases, none of the charged tracks faking the displaced vertex are real electrons or muons. Our simulation finds approximately 3500 such background events are expected to fake the signal event topology before running the PID system; these can be safely rejected as long as the fake rate of the PID is lower than $\sim 2\%$ per particle species.

There are potentially important backgrounds from a variety of possible sources:

- **Real lepton + fake hadron:** processes involving one real electron or muon and a second charged particle produced together from a common displaced vertex (e.g. $K^0 \to \pi^+ e^- \bar{\nu}_e$ or $\Lambda \to p e^- \bar{\nu}_e$) can fake our signal if the charged hadron is misidentified as an electron or muon. Using the same simulation details described above, we find that MUonE can expect approximately ~ 6 SM events for $\sim 10^{16}$

muons on target, and these can be safely rejected using PID as long as the per-particle fake rate is lower than 18%.

- **Real dileptons:** there are also SM processes that result in displaced $e^+ e^-$ pairs with displaced vertices (e.g. $K^0 \to \pi^0 \pi^0$ with one $\pi^0 \to e^+ e^- \gamma$ decay), which also fakes our signal topology. However, such a production processes are always accompanied by high-energy photons (coming from the $\pi^0 \to e^+ e^- \gamma$ decay and from the other π^0 decay in the event), so these processes can be efficiently vetoed; our simulation shows that no such background events passed our selection criteria. This conclusion is consistent with the results of Ref. [10], which found similarly low SM backgrounds for MUonE sensitivity to new forces.

- **QED hadroproduction:** finally, electromagnetic muon-nucleus scattering can occasionally produce a K^0 or Λ to fake our signal via $\mu N \to \mu N \gamma^* (\gamma^* \to \bar{q}q)$. This process, however, is suppressed by both the production cross section and the branching ratio for the $\bar{q}q$ to combine into a K^0 or a Λ. We estimate that such processes contribute less than 1 event per 10^{16} muons on target.

Based on these considerations, we conclude that SM backgrounds are negligible for our selection criteria.

Results and Discussion. In Fig. 6 we present our main results, which demonstrate that, for a design $\mu - \text{Be}$ luminosity of 4.7×10^3 pb^{-1}[6], MUonE (solid red curve) can probe much of the parameter space compatible with thermal freeze out (solid black curve) for a variety of different mass splittings. Our projection is defined with a 95% confidence interval using the event selection criteria from Table I. For these results, we assume that SM

---

[5] For muon-Be scattering, the inclusive soft QCD cross section is $\sigma \approx 8.2 \times 10^5$ pb, while the inclusive DIS cross section is $\sigma \approx 3.4 \times 10^4$ pb, where the separation between these regimes is defined at the threshold momentum transfer $Q^2 = (2 \text{ GeV})^2$

[6] The total $\mu - \text{Be}$ luminosity is smaller than the luminosity for $\mu - e$ scattering by a factor of $1/4$. We further divide this number by 8 since we only use the last 5 (out of 40) modules.
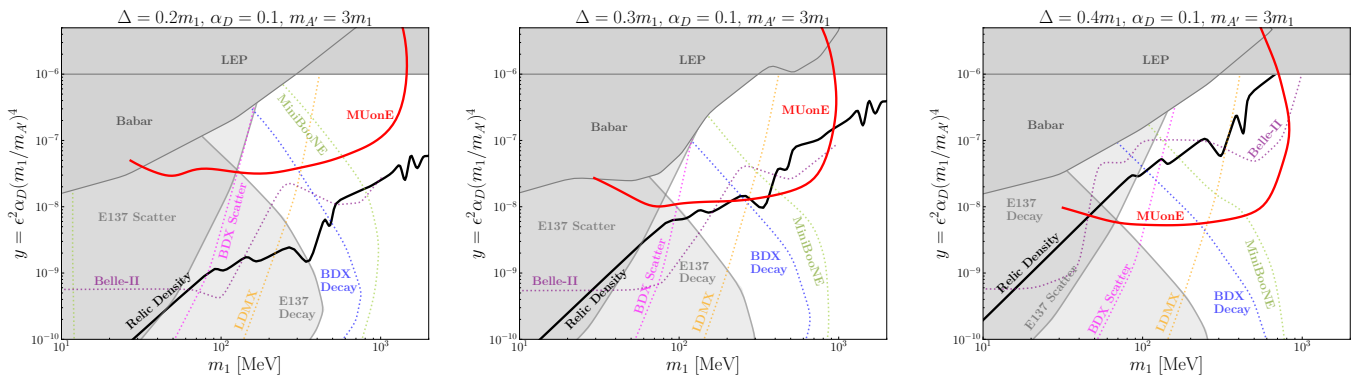
FIG. 6. Projected inelastic DM sensitivity at the MUonE experiment (red curve) for a variety of mass splittings assuming a muon luminosity of 4.7×10^3 pb^{-1}. Along the black curve, the DM achieves the observed relic density through $\chi_1\chi_2$ coannihilation [15]. The gray-shaded regions are excluded by BABAR [39], LEP [40], and E137 [41] – the exclusion regions for BABAR and E137 are based on the reinterpretation in [20]. The dashed curves stand for projected limits from BDX [42], LDMX [3], MiniBooNE [43] and Belle II [44], also computed in Ref. [20].

backgrounds are negligible, which is justified by our background simulation described above. Also shown are existing limits from BaBar and E137 computed in Ref. [20].

The shaded gray regions in Fig. 6 represent existing limits on this scenario from the BaBar monophoton search [20, 39], the E137 electron beam dump search for long lived particles [20, 41], and LEP precision electroweak constraints on kinetically mixed dark photons [40]. The dashed curves represent future projections for BDX [42, 45]], LDMX [3, 15, 46], MiniBooNE [20, 43], and Belle II [20, 47]

In summary, we have shown that the MUonE experiment can powerfully probe thermal relic dark matter in models with inelastic mass splittings. In such models, dark states are produced in muon-beryllium scattering and the heavier state decays semi-visibly to yield a displaced dilepton pair downstream of the target. Our approach is fully parasitic with the proposed MUonE experimental setup and requires no additional equipment. Furthermore, our results demonstrate the importance of the MUonE ECAL system, which is currently at risk of

being eliminated from the experimental design [48]. In our search, the ECAL plays an essential role in rejecting SM backgrounds for the dark matter signal and expanding the MUonE experimental program. Thus, we strongly encourage the collaboration to keep this component as part of the full setup.

[1] P. deNiverville, C.-Y. Chen, M. Pospelov, and A. Ritz, "Light dark matter in neutrino beams: production modelling and scattering signatures at MiniBooNE, T2K and SHiP," *Phys. Rev. D* **95** no. 3, (2017) 035006, arXiv:1609.01770 [hep-ph].

[2] E. Izaguirre, G. Krnjaic, and M. Pospelov, "MeV-Scale Dark Matter Deep Underground," *Phys. Rev. D* **92** no. 9, (2015) 095014, arXiv:1507.02681 [hep-ph].

[3] **LDMX** Collaboration, T. Åkesson *et al.*, "Light Dark Matter eXperiment (LDMX)," arXiv:1808.05219 [hep-ex].

[4] **NA64** Collaboration, Y. M. Andreev *et al.*, "First Results in the Search for Dark Sectors at NA64 with

the CERN SPS High Energy Muon Beam," *Phys. Rev. Lett.* **132** no. 21, (2024) 211803, arXiv:2401.01708 [hep-ex].

[5] S. Gori *et al.*, "Dark Sector Physics at High-Intensity Experiments," arXiv:2209.04671 [hep-ph].

[6] M. Battaglieri *et al.*, "US Cosmic Visions: New Ideas in Dark Matter 2017: Community Report," in *U.S. Cosmic Visions: New Ideas in Dark Matter*. 7, 2017. arXiv:1707.04591 [hep-ph].

[7] G. Abbiendi *et al.*, "Measuring the leading hadronic contribution to the muon g-2 via μe scattering," *Eur. Phys. J. C* **77** no. 3, (2017) 139, arXiv:1609.08987 [hep-ex].

[8] G. Abbiendi, "Letter of intent: the muone project," Tech. Rep. CERN-SPSC-2019-026, SPSC-I-252, CERN, Geneva, Jun, 2019. https://cds.cern.ch/record/2677471.

[9] **Muon g-2** Collaboration, G. W. Bennett *et al.*, "Final Report of the Muon E821 Anomalous Magnetic Moment Measurement at BNL," *Phys. Rev. D* **73** (2006) 072003, arXiv:hep-ex/0602035.

[10] I. Galon, D. Shih, and I. R. Wang, "Dark photons and displaced vertices at the MUonE experiment," *Phys. Rev. D* **107** no. 9, (2023) 095003, arXiv:2202.08843 [hep-ph].

[11] K. Asai, K. Hamaguchi, N. Nagata, S.-Y. Tseng, and J. Wada, "Probing the Lμ-Lτ gauge boson at the MUonE experiment," *Phys. Rev. D* **106** no. 5, (2022) L051702, arXiv:2109.10093 [hep-ph].

[12] G. Grilli di Cortona and E. Nardi, "Probing light mediators at the MUonE experiment," *Phys. Rev. D* **105** no. 11, (2022) L111701, arXiv:2204.04227 [hep-ph].

[13] D. Tucker-Smith and N. Weiner, "Inelastic dark matter," *Phys. Rev. D* **64** (2001) 043502, arXiv:hep-ph/0101138.

[14] M. Carrillo González and N. Toro, "Cosmology and signals of light pseudo-Dirac dark matter," *JHEP* **04** (2022) 060, arXiv:2108.13422 [hep-ph].

[15] A. Berlin, N. Blinov, G. Krnjaic, P. Schuster, and N. Toro, "Dark Matter, Millicharges, Axion and Scalar Particles, Gauge Bosons, and Other New Physics with LDMX," *Phys. Rev. D* **99** no. 7, (2019) 075001, arXiv:1807.01730 [hep-ph].

[16] A. Berlin and F. Kling, "Inelastic Dark Matter at the LHC Lifetime Frontier: ATLAS, CMS, LHCb, CODEX-b, FASER, and MATHUSLA," *Phys. Rev. D* **99** no. 1, (2019) 015021, arXiv:1810.01879 [hep-ph].

[17] J. R. Jordan, Y. Kahn, G. Krnjaic, M. Moschella, and J. Spitz, "Signatures of Pseudo-Dirac Dark Matter at High-Intensity Neutrino Experiments," *Phys. Rev. D* **98** no. 7, (2018) 075020, arXiv:1806.05185 [hep-ph].

[18] **Planck** Collaboration, N. Aghanim *et al.*, "Planck 2018 results. VI. Cosmological parameters," *Astron. Astrophys.* **641** (2020) A6, arXiv:1807.06209 [astro-ph.CO]. [Erratum: Astron.Astrophys. 652, C4 (2021)].

[19] E. Izaguirre, G. Krnjaic, and B. Shuve, "Discovering Inelastic Thermal-Relic Dark Matter at Colliders," *Phys. Rev. D* **93** no. 6, (2016) 063523, arXiv:1508.03050 [hep-ph].

[20] E. Izaguirre, Y. Kahn, G. Krnjaic, and M. Moschella, "Testing Light Dark Matter Coannihilation With Fixed-Target Experiments," *Phys. Rev. D* **96** no. 5, (2017) 055007, arXiv:1703.06881 [hep-ph].

[21] S. R. Amendolia *et al.*, "A Measurement of the Pion Charge Radius," *Phys. Lett. B* **146** (1984) 116–120.

[22] **NA7** Collaboration, S. R. Amendolia *et al.*, "A Measurement of the Space - Like Pion Electromagnetic Form-Factor," *Nucl. Phys. B* **277** (1986) 168.

[23] S. Borsanyi *et al.*, "Leading hadronic contribution to the muon magnetic moment from lattice QCD," *Nature* **593** no. 7857, (2021) 51–55, arXiv:2002.12347 [hep-lat].

[24] **CMD-3** Collaboration, F. V. Ignatov *et al.*, "Measurement of the e+e-→π+π- cross section from threshold to 1.2 GeV with the CMD-3 detector," *Phys. Rev. D* **109** no. 11, (2024) 112002, arXiv:2302.08834

[25] T. Aoyama *et al.*, "The anomalous magnetic moment of the muon in the Standard Model," *Phys. Rept.* **887** (2020) 1–166, arXiv:2006.04822 [hep-ph].

[26] A. Boccaletti *et al.*, "High precision calculation of the hadronic vacuum polarisation contribution to the muon anomaly," arXiv:2407.10913 [hep-lat].

[27] **Muon g-2** Collaboration, B. Abi *et al.*, "Measurement of the Positive Muon Anomalous Magnetic Moment to 0.46 ppm," *Phys. Rev. Lett.* **126** no. 14, (2021) 141801, arXiv:2104.03281 [hep-ex].

[28] **Muon g-2** Collaboration, D. P. Aguillard *et al.*, "Measurement of the Positive Muon Anomalous Magnetic Moment to 0.20 ppm," *Phys. Rev. Lett.* **131** no. 16, (2023) 161802, arXiv:2308.06230 [hep-ex].

[29] E. Spedicato, "Status of the MUonE experiment," *Nuovo Cim. C* **47** no. 3, (2024) 138.

[30] **CMS** Collaboration, "The Phase-2 Upgrade of the CMS Tracker," Tech. Rep. CERN-LHCC-2017-009, CMS-TDR-014, CERN, Geneva, 2017. https://cds.cern.ch/record/2272264.

[31] **CMS** Collaboration, E. Migliore, "Status of the upgrade project of the CMS Tracker for HL-LHC," Tech. Rep. 10, CERN, Geneva, 2022. https://cds.cern.ch/record/2797715.

[32] U. Marconi and C. Matteuzi, "Private communication." 2021.

[33] R. Walters, "Stopping-power & range tables for electrons, protons, and helium ions," *NIST Standard Reference Database 124, NIST* (2017) .

[34] **Particle Data Group** Collaboration, R. L. Workman and Others, "Review of Particle Physics," *PTEP* **2022** (2022) 083C01.

[35] A. Alloul, N. D. Christensen, C. Degrande, C. Duhr, and B. Fuks, "FeynRules 2.0 - A complete toolbox for tree-level phenomenology," *Comput. Phys. Commun.* **185** (2014) 2250–2300, arXiv:1310.1921 [hep-ph].

[36] A. Belyaev, N. D. Christensen, and A. Pukhov, "CalcHEP 3.4 for collider physics within and beyond the Standard Model," *Comput. Phys. Commun.* **184** (2013) 1729–1769, arXiv:1207.6082 [hep-ph].

[37] C.-Y. Chen, M. Pospelov, and Y.-M. Zhong, "Muon Beam Experiments to Probe the Dark Sector," *Phys. Rev. D* **95** no. 11, (2017) 115005, arXiv:1701.07437 [hep-ph].

[38] C. Bierlich *et al.* *SciPost Physics Codebases* (3, 2022) , arXiv:2203.11601 [hep-ph].

[39] **BaBar** Collaboration, B. Aubert *et al.*, "Searches for Lepton Flavor Violation in the Decays τ + → e+γ and τ + → M+γ," *Phys. Rev. Lett.* **104** (2010) 021802, arXiv:0908.2381 [hep-ex].

[40] A. Hook, E. Izaguirre, and J. G. Wacker, "Model Independent Bounds on Kinetic Mixing," *Adv. High Energy Phys.* **2011** (2011) 859762, arXiv:1006.0973 [hep-ph].

[41] J. D. Bjorken, S. Ecklund, W. R. Nelson, A. Abashian, C. Church, B. Lu, L. W. Mo, T. A. Nunamaker, and P. Rassmann, "Search for Neutral Metastable Penetrating Particles Produced in the SLAC Beam Dump," *Phys. Rev. D* **38** (1988) 3375.

[42] **BDX** Collaboration, M. Battaglieri *et al.*, "Dark Matter Search in a Beam-Dump eXperiment (BDX) at Jefferson Lab," arXiv:1607.01390 [hep-ex].

[43] **MiniBooNE DM** Collaboration, A. A.

Aguilar-Arevalo *et al.*, "Dark Matter Search in Nucleon, Pion, and Electron Channels from a Proton Beam Dump with MiniBooNE," *Phys. Rev. D* **98** no. 11, (2018) 112004, `arXiv:1807.06137 [hep-ex]`.

[44] **Belle** Collaboration, K. Uno, K. Hayasaka, *et al.*, "Search for lepton-flavor-violating tau-lepton decays to $\ell\gamma$ at Belle," *JHEP* **10** no. 10, (2021) 19, `arXiv:2103.12994 [hep-ex]`.

[45] E. Izaguirre, G. Krnjaic, P. Schuster, and N. Toro, "New Electron Beam-Dump Experiments to Search for MeV to few-GeV Dark Matter," *Phys. Rev. D* **88** (2013) 114015, `arXiv:1307.6554 [hep-ph]`.

[46] E. Izaguirre, G. Krnjaic, P. Schuster, and N. Toro, "Testing GeV-Scale Dark Matter with Fixed-Target Missing Momentum Experiments," *Phys. Rev. D* **91** no. 9, (2015) 094026, `arXiv:1411.1404 [hep-ph]`.

[47] **Belle-II** Collaboration, W. Altmannshofer *et al.*, "The Belle II Physics Book," *PTEP* **2019** no. 12, (2019) 123C01, `arXiv:1808.10567 [hep-ex]`. [Erratum: PTEP 2020, 029201 (2020)].

[48] Y. Ulrich, "Private communication." 2024.